

EQUATION OF STATE OF NUCLEONIC MATTER* **

W. CASSING†

Institut für Theoretische Physik, Universität Giessen
D-35392 Giessen, Germany*(Received November 16, 1999)*

The nuclear equation of state (EoS) is investigated by flow phenomena in relativistic heavy-ion collisions, both in transverse and radial direction, in comparison to experimental data from 150 A MeV to 11 A GeV. To this aim the collective dynamics of the nucleus–nucleus collision is described within a transport model of the coupled channel RBUU type. There are two factors which dominantly determine the baryon flow at these energies: the momentum dependence of the scalar (U_S) and vector potentials (U_μ) for baryons and the resonance/string degrees of freedom for energetic hadron excitations. We fix the explicit momentum dependence of the nucleon–meson couplings by the nucleon optical potential up to 1 GeV and extrapolate to higher energy. When assuming the optical potential to vanish identically for $E_{\text{kin}} \geq 3.5$ GeV we simultaneously describe the sideward flow data of the PLASTIC BALL, FOPI, EoS and E877 collaborations, the elliptic flow data of the E895 and E877 collaborations and approximately the rapidity and transverse mass distribution of protons at AGS energies without employing any *explicit* assumption on a phase transition in the EoS. However, the gradual change from hadronic to string degrees of freedom with increasing bombarding energy can be viewed as a transition from *hadronic* to *string* matter, *i.e.* a dissolution of hadrons at high energy density.

PACS numbers: 21.65.+f, 25.75.-q, 25.75.Ld

* Invited talk presented at the XXVI Mazurian Lakes School of Physics, Krzyże, Poland, September 1-11, 1999.

** Supported by BMBF and GSI Darmstadt.

† In collaboration with A. Hombach, U. Mosel and P. K. Sahu.

1. Introduction

Relativistic heavy-ion collisions (RHIC) provide a unique tool to study nuclear matter at high densities and temperatures, reminiscent of the early big-bang of the universe, but with better statistics and under controlled conditions. These reactions also provide constraints on the interior of neutron stars, where the nuclear equation-of-state (EoS) plays an essential role for the possible existence of an inner quark core or an extended mixed phase of quarks and hadrons [1]. However, since in a RHIC the system initially is far away from thermal and chemical equilibrium, both particle production and collective motion depend on various quantities such as the stiffness of the EoS, the momentum dependence of the interaction or mean-field potentials (MDI), in-medium modifications of the NN cross section σ_{NN} , the initial momentum distribution of the nucleons [2,3] as well as the number of hadronic degrees of freedom accounted for in the transport simulation [4]. It is thus necessary not to focus on a single observable alone but to investigate the dynamical evolution of the RHIC within a single model that is able to describe all relevant single-particle as well as collective quantities.

Whereas the experimental and theoretical studies of collective nuclear flow have been restricted to the 1–2 A GeV energy regime in the past [5,6], more recently both the directed transverse flow (sideward flow) and the flow tensor (elliptic flow) have been measured and reported by the BNL-E877 collaboration [7–10] for heavy-ion (Au+Au) collisions at AGS energies in the energy range of $1 \text{ A GeV} \leq E_{\text{inc}} \leq 11 \text{ A GeV}$. In this energy range the directed transverse flow first grows, saturates at around 2 A GeV, and then decreases experimentally with energy showing no minimum as expected from hydrodynamical calculations including a first order phase transition in the EoS [11]. Whether this decrease in directed flow or the change of sign in elliptic flow is indicative of a phase transition [12] is a question of high current interest.

In this contribution the collective behaviour of nuclear matter in a heavy-ion collision is reviewed in the energy range from 150 A MeV to 11 A GeV for various systems using the transport model [13]. For energies above 1 A GeV it has been, furthermore, complemented by the string dynamics from the HSD transport approach [14] which has been tested extensively for $p + A$ and $A + A$ collisions from SIS to SPS energies [15].

2. The extended RBUU-model

To describe the heavy-ion collision data at energies starting from the SIS at GSI to the SPS regime at CERN, relativistic transport models have been extensively used [14,16–19]. For a general derivation of transport theories the reader is referred to Ref. [20] and to Ref. [15] for a recent review. Among these

transport models the Relativistic Boltzmann–Uehling–Uhlenbeck (RBUU) approach incorporates the relativistic mean-field (RMF) theory, which is applicable also to various nuclear structure problems as well as for neutron star studies [1, 21]. Since it is based on an effective hadronic Lagrangian density it allows to evaluate directly the nuclear EoS at zero and finite nuclear temperature T as well as the scalar and vector mean fields U_S and U_μ , that determine the in-medium particle properties, for arbitrary configurations of nucleons in phase space [20]. Here we essentially base the studies on the Lagrangian (parameter set NL3) from Ref. [22] since this Lagrangian has been applied widely in the analysis of heavy-ion collisions by various groups [13, 23, 24].

We recall that the most simple versions of RMF theories assume the scalar and vector fields to be represented by point-like meson–baryon couplings. These couplings lead to a linearly growing Schrödinger-equivalent potential in nuclear matter as a function of the kinetic energy E_{kin} , which naturally explains the energy dependence of the nucleon optical potential at low energies (≤ 200 MeV). However, a simple RMF does not describe the nucleon optical potential at higher energies, where it deviates substantially from a linear function and saturates at $E_{\text{kin}} \approx 1$ GeV [25]. Since the energy dependence of sideward flow is controlled in part by the nucleon optical potential, the simple RMF cannot be applied to high-energy heavy-ion collisions. In order to remedy this aspect, the more sophisticated RBUU approaches invoke an explicit momentum dependence of the coupling constant, *i.e.* a form factor for the meson–baryon couplings [14, 15, 26].

Further important ingredients at AGS energies are the resonance/string degrees of freedom which are excited during the reaction in high energy baryon–baryon or meson–baryon collisions. While at SIS energies particle production mainly occurs through baryon resonance production and their decay, the string phenomenology is found to work well at SPS energies (≈ 200 A GeV) [15]. One of the characteristic features of the AGS energy regime is the competition between these two particle production mechanisms which might be separated by some energy scale $\sqrt{s_{sw}}$ [27]. Due to this complexity there are various ways to implement elementary cross sections in transport models [4, 12, 15, 23, 24, 28]. One of the extremes is to parameterize all possible cross sections directly for multi-pion production, $NN \rightarrow NNn\pi$ ($n \geq 3$) only through N, Δ, π degrees of freedom; the other extreme is to fully apply string phenomenology in this energy region without employing any resonances. Although it is possible to reproduce the elementary cross sections from NN and πN collisions and the inclusive final hadron spectra in heavy-ion collisions within these different models, we expect that differences should appear in the dynamical evolution of the system, *e.g.* in the thermodynam-

ical properties [4, 29] and in collective flow [27]. For example, if thermal equilibrium is achieved at a given energy density, models with a larger number of degrees of freedom including strings will give smaller temperature and pressure [30].

We have employed here the combination of a resonance production model [31] and the Lund string model [32] as incorporated in the Hadron–String–Dynamics (HSD) approach [14, 15]. In the practical implementation for NN or MN collisions at invariant energies lower (higher) than a threshold energy $\sqrt{s_{sw}}$ resonances (strings) are assumed to be excited (see below).

2.1. The optical potential

In this presentation the scalar and vector mean fields U_S and U_μ are calculated on the basis of the same Lagrangian density as considered in Ref. [13], which contains nucleon, σ and ω meson fields and nonlinear self-interactions of the scalar field (*cf.* NL3 parameter set [22]). The scalar and vector form factors at the vertices are taken into account in the form [14]

$$f_s(p) = \frac{\Lambda_s^2 - \frac{1}{2}p^2}{\Lambda_s^2 + p^2} \quad \text{and} \quad f_v(p) = \frac{\Lambda_v^2 - \frac{1}{6}p^2}{\Lambda_v^2 + p^2}, \quad (1)$$

where the cut-off parameters $\Lambda_s = 1.0$ GeV and $\Lambda_v = 0.9$ GeV are obtained by fitting the Schrödinger equivalent potential,

$$U_{\text{sep}}(E_{\text{kin}}) = U_s + U_0 + \frac{1}{2M}(U_s^2 - U_0^2) + \frac{U_0}{M}E_{\text{kin}}, \quad (2)$$

to Dirac phenomenology for intermediate energy proton–nucleus scattering [25].

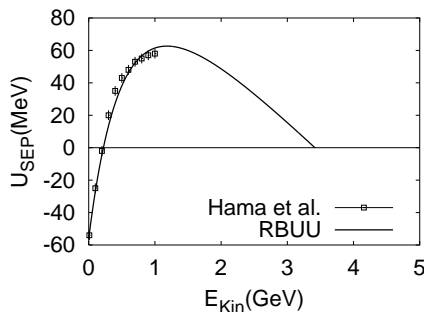


Fig. 1. The Schrödinger equivalent potential (2) at density ρ_0 as a function of the nucleon kinetic energy E_{kin} . The solid curve (RBUU) results from the momentum-dependent potentials discussed in the text. The data points are from Hama *et al.* [25].

The resulting Schrödinger equivalent potential (2) is shown in Fig. 1 as a function of the nucleon kinetic energy with respect to the nuclear matter at rest in comparison to the data from Hama *et al.* [25] (open squares). The experimental increase of the Schrödinger equivalent potential up to $E_{\text{kin}} = 1$ GeV is described quite well; then the potential decreases and is set to zero above 3.5 GeV.

For the transition rate in the collision term of the transport model we employ in-medium cross sections as in Ref. [31] that are parameterized in line with the corresponding experimental data for $\sqrt{s} \leq \sqrt{s_{sw}}$. For higher invariant collision energies we adopt the Lund string formation and fragmentation model [32] as incorporated in the HSD transport approach [14] which has been used extensively for the description of particle production in nucleus–nucleus collisions from SIS to SPS energies [15]. In the present relativistic transport approach (RBUU) as in Ref. [13] we explicitly propagate nucleons and Δ 's as well as all baryon resonances up to a mass of 2 GeV with their isospin degrees of freedom [31,33]. Furthermore, $\pi, \eta, \rho, \omega, K, \bar{K}$ and σ mesons are propagated, too, where the σ is a short lived effective resonance that describes s -wave $\pi\pi$ scattering. For more details we refer the reader to Refs. [31,33] concerning the low energy cross sections and to Refs. [14,15] with respect to the implementation of the string dynamics.

2.2. Transverse mass spectra of protons

In Fig. 2 we show the dependence of the calculated proton transverse mass spectra in a central collision of Au+Au at 11.6 A GeV for $b < 3.5$ fm for $\sqrt{s_{sw}} = 2.6$ GeV (dotted histograms) and 3.5 GeV (solid histograms) in comparison to the experimental data of the E802 collaboration [34]. A cascade calculation (crosses) is shown additionally for $\sqrt{s_{sw}} = 3.5$ GeV to demonstrate the effect of the mean-field potentials which lead to a reduction of the transverse mass spectra below 0.3 GeV. As expected, the transverse mass spectrum is softer for smaller $\sqrt{s_{sw}}$ due to the larger number of degrees of freedom in the string model relative to the resonance model.

We note that strings may be regarded as hadronic excitations in the continuum of lifetime $t_F \approx 0.8$ fm/c (in their rest frame) that take over a significant part of the incident collision energy by their invariant mass. They decay dominantly to light baryons and mesons and only to a low extent to heavy baryon resonances. Thus the number of particles for fixed system time is larger for string excitations than for the resonance model where several hadrons propagate as a single heavy resonance which might be regarded as a cluster of a nucleon + n pions. As a consequence the translational energies are suppressed in string excitations and, as a result, the temperature as well as the pressure are smaller when exciting strings.

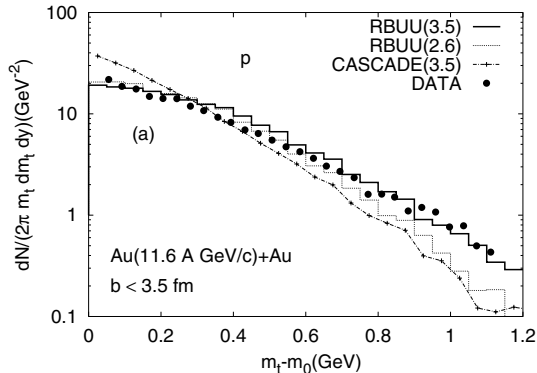


Fig. 2. The transverse mass spectra of protons for Au+Au collisions at $b < 3.5$ fm. The solid line and the dot-dashed line with crosses are results for $\sqrt{s_{sw}}=3.5$ GeV with and without nuclear potentials, respectively. The dotted line RBUU(2.6) is for $\sqrt{s_{sw}}=2.6$ GeV. The data points are taken from the E802 collaboration [34].

From the above comparison with the experimental transverse mass spectra for protons we find $\sqrt{s_{sw}} \approx 3.5$ GeV, which implies that binary final baryon channels should dominate up to $\sqrt{s} \approx 3.5$ GeV which corresponds to a proton laboratory energy of about 4.6 GeV for pp collisions.

3. SIS energies

3.1. Transverse flow

Within the RBUU model described above we now calculate the transverse flow for various systems and beam energies and analyse the dependence on different quantities. The flow F is defined as the slope of the transverse momentum distribution at midrapidity,

$$F = \frac{d\langle p_x \rangle}{dy} \Big|_{y=y_0}, \quad (3)$$

which is essentially generated by the *participating* matter in the ‘fireball’ [4]. The latter finding explains why flow does not clearly distinguish between an EoS with and without momentum-dependent forces. Since the fireball contains the stopped matter, the relative momenta in the fireball (besides the unordered thermal motion) are small. Only when applying additional cuts, *e.g.* on high transverse momenta [16, 18], *i.e.* by selecting particles escaping early from the fireball, or selecting mainly participant or spectator particles by appropriate Θ_{cm} -Cuts [35], a difference between the momentum-dependent and momentum-independent EoS can be established.

The FOPI data on proton flow [7] indicate a decrease of sideways flow above 1 A GeV incident energy following the well known logarithmic increase at low energies. Using standard potential parameterizations, both nonrelativistic [2] and relativistic [13], this behavior cannot be understood within conventional transport models. In the latter the optical potential stays constant or even increases at high momenta and therefore the repulsion generated from the momentum-dependent forces in a HIC gives rise to a significant contribution to the flow signal. However, since the nucleon–nucleus optical potential is only known up to 1 GeV experimentally [25], it was proposed that this decrease of flow above 1 A GeV might indicate a decrease of the optical potential at high relative momenta or at high baryon density [13].

In Ref. [3] the transverse momentum of the baryons has been disentangled into a collisional part, a mean-field part and a part originating from the Fermi-motion of the particles,

$$p_t = p_t^{\text{coll}} + p_t^{\text{MF}} + p_t^{\text{Fermi}}, \quad (4)$$

where p_t^{Fermi} practically does not contribute at midrapidity. Thus disentangling the flow signal into a collisional and a potential part, it turns out that $\sim 50\%$ of the flow stems from the particle–particle collisions while roughly another 50% are generated by the potential repulsion at 1 A GeV. Fig. 3 shows these two contributions for flow for the system Ni+Ni at $b = 4$ fm in comparison to the experimental data using different EoS denoted by ‘hard’, ‘medium’ and ‘soft’. Both the collisional “background” and the potential part rise up to 1 A GeV incident energy and remain constant above, whereas the

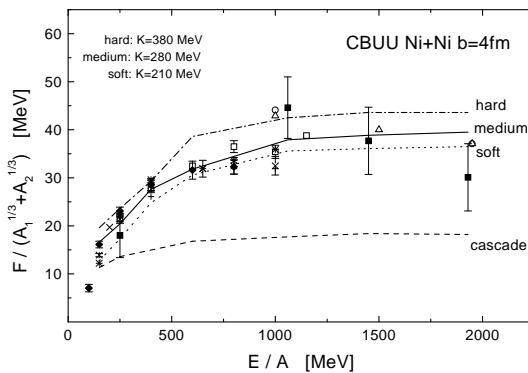


Fig. 3. Transverse flow for a Ni+Ni collision at $b = 4$ fm as calculated within the RBUU model in cascade mode (dashed lower line) and for equations of state with different compressibilities K in comparison to data from EOS, Plastic Ball and FOPI as compiled by Ref. [7].

data indicate a decrease above 1 A GeV. As seen from Fig. 3 the Ni+Ni data are described reasonably by both a ‘soft’ and ‘medium’ EoS, while a cascade calculation fails substantially.

A note of caution has to be added here: The flow F (3) not only depends on the baryon self-energies U_S and U_μ but also on the number of (resonance) degrees of freedom above about 1 A GeV as first pointed out by Hombach *et al.* [4]. This observation will become crucial at AGS energies.

3.2. Radial flow

Radial flow has been discovered [36] when analyzing the flow pattern of very central events of RHIC. In contrast to transverse flow up to about 70 % of the incident energy (stored in the hot compressed fireball) is released as ordered radial expansion of the nuclear matter. Thus the hope is to extract information especially on the compressibility of the EoS via the magnitude of the radial flow.

Experimentally the radial flow is characterized or fitted in terms of the Siemens–Rasmussen formula [37]

$$\frac{d^3 N}{dE d^2 \Omega} \sim p \cdot e^{-\gamma E/T} \left\{ \frac{\sinh \alpha}{\alpha} \cdot (\gamma E + T) - T \cdot \cosh \alpha \right\} \quad (5)$$

with $\gamma = (1 - \beta^2)^{-1/2}$ and $\alpha = \gamma \beta p/T$, while β denotes the flow velocity and T characterizes some temperature. We follow the same strategy in our RBUU calculations and apply a least square fit to the RBUU nucleon spectra using Eq. (5).

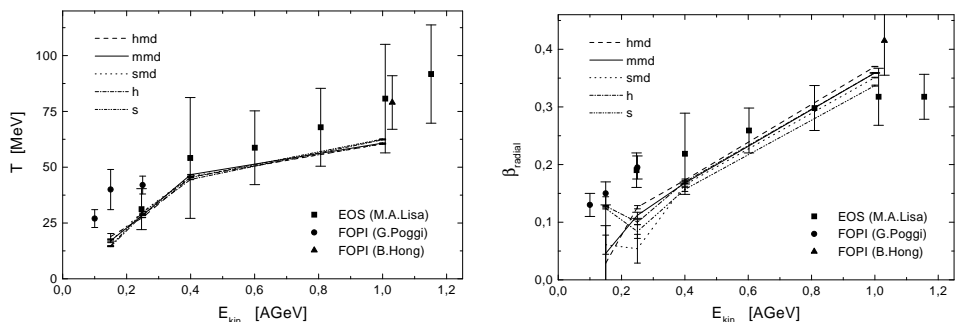


Fig. 4. The temperature (l.h.s.) and radial flow velocity (r.h.s.) for central Au+Au collisions evaluated via Eq. (5) from the RBUU calculations in comparison to the experimental data from Refs. [38–40]. The symbol ‘s’ denotes a soft EoS without momentum dependent forces, ‘h’ a hard EoS and ‘smd’, ‘mmd’ and ‘hmd’ correspond to a soft, medium and hard momentum dependent EoS, respectively.

The results of the RBUU calculations for central Au+Au collisions are shown in Fig. 4 as a function of the bombarding energy in comparison to the data from [38–40]. We find that the ‘temperature’ T is systematically under-predicted in all schemes investigated (soft and hard EoS, with and without momentum dependent forces), and that the flow velocities are not correctly reproduced, being too low at low energy and crossing the experimental data around 800 A MeV. This might indicate a strong binding from the potential which gives not enough repulsion at high densities and overcompensates the collisional pressure from the fireball. However, the nucleon spectra resulting from the RBUU calculation show a strong non-thermal component at low incident energies and are thus in contradiction to the physical picture behind Eq. (5) which assumes an isentropic expansion of a thermal equilibrated source. In Ref. [41] the degree of equilibration in a HIC has been investigated as a function of the incident energy and the system mass and it has been found that even the most massive systems like Au+Au do not equilibrate at low energies.

4. AGS energies

4.1. Sidewards flow

We now turn to the AGS energy regime from 1–11 AGeV. The calculations are performed for the impact parameter $b = 6 fm$ for Au+Au systems, since for this impact parameter we get the maximum flow which corresponds to the multiplicity bins $M3$ and $M4$ as defined by the Plastic Ball collaboration [42] at BEVALAC/SIS energies. In Fig. 5 (l.h.s.) the transverse flow (3) is displayed in comparison to the data from Refs. [7, 8, 43] for Au+Au systems. The solid line (RBUU with $\sqrt{s_{sw}} = 3.5$ GeV) is obtained with the scalar and vector self energies as discussed above, Eq. (1). The dotted line (CASCADE with $\sqrt{s_{sw}} = 3.5$ GeV) corresponds to cascade calculations for reference in order to show the effect of the mean field relative to that from collisions. We observe that the solid line (RBUU, *cf.* Fig. 1) is in good agreement with the flow data [43] at all energies; above bombarding energies of 6 A GeV the results are practically identical to the cascade calculations showing the potential effects to cancel out.

We note that the sideward flow shows a maximum around 2 A GeV for Au+Au and decreases continuously at higher beam energy (≥ 2 A GeV) without showing any explicit minimum as in Ref. [11]. This is due to the fact that the repulsive force caused by the vector mean field decreases at high beam energies (*cf.* Fig. 1) such that in the initial phase of the collision there are no longer strong gradients of the potential within the reaction plane. In subsequent collisions, which are important for Au+Au due to the system size, the kinetic energy of the particles relative to the local rest frame is then

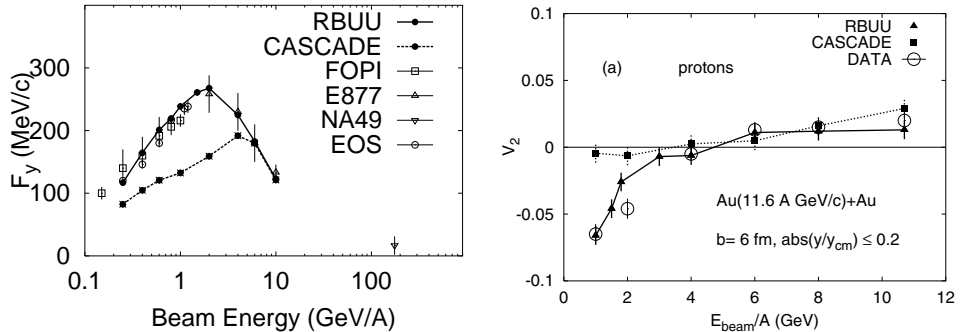


Fig. 5. (l.h.s.) The sideward flow $F(y)$ as a function of the beam energy per nucleon for Au+Au collisions at $b = 6$ fm from the RBUU calculations. The solid line results for the parameter set RBUU, the dotted line for a cascade calculation with $\sqrt{s_{sw}} = 3.5$ GeV. The data points are from the FOPI and EoS Collaborations [7, 43]. (r.h.s.) The elliptic flow v_2 of protons versus the beam energy per nucleon for Au+Au collisions at $b = 6$ fm from the RBUU calculations. The solid line results for the parameter set RBUU, the dotted line for a cascade calculation with $\sqrt{s_{sw}} = 3.5$ GeV. The data points are from the EoS Collaboration [9, 10].

in a range ($E_{\text{kin}} \leq 1$ GeV) where the Schrödinger equivalent potential (at density ρ_0) is determined by the experimental data [25]. We thus conclude that for the sideward flow data up to 11 A GeV one needs a considerably strong vector potential at low energy and that one has to reduce the vector mean field at high beam energy in line with Fig. 1. In other words, there is only a weak repulsive force at high relative momenta or high densities.

Another aspect of the decreasing sideward flow can be related to the dynamical change in the resonance/string degrees of freedom as already discussed above. For instance, for $\sqrt{s_{sw}} = 2.6$ GeV the calculated flow turns out to be smaller than the data above 1.5 A GeV and approaches the cascade limit already for ≈ 3 –4 A GeV. This is due to the fact that in strings the incident energy is stored to a larger extent in their masses and the translational energy is reduced accordingly.

4.2. Elliptic flow

Apart from the in-plane flow of protons the out-of-plane collective flow provides additional information and constraints on the nuclear potentials involved. In this respect the elliptic flow for protons

$$v_2 = \langle (P_x^2 - P_y^2) / (P_x^2 + P_y^2) \rangle \quad (6)$$

for $|y/y_{\text{cm}}| \leq 0.2$ is shown in Fig. 5 (r.h.s.) as a function of incident energy for Au+Au collisions at $b = 6$ fm. The solid line (RBUU with $\sqrt{s_{sw}} = 3.5$

GeV) is obtained with the same mean fields as discussed before while the dotted line (CASCADE with $\sqrt{s_{sw}} = 3.5$ GeV) stands again for the cascade results. The flow parameter v_2 changes its sign from negative at low energies ($\leq 5A$ GeV) to positive elliptic flow at high energies ($\geq 5A$ GeV).

This can be understood as follows: At low energies the squeeze-out of nuclear matter leads to a negative elliptic flow since projectile and target spectators distort the collective expansion of the ‘fireball’ in the reaction plane. At high energies the projectile and target spectators do not hinder anymore the in-plane expansion of the ‘fireball’ due to their high velocity ($\approx c$); the elliptic flow then is positive. The competition between squeeze-out and in-plane elliptic flow at AGS energies depends on the nature of the nuclear force as pointed out already by Danielewicz *et al.* [12]. We note, however, that in our calculation with the momentum-dependent potential (Fig. 1) we can describe both the sideward as well as elliptic flow data [9,10] simultaneously without incorporating any phase transition in the EOS as in Ref. [12].

In the cascade calculation the elliptic flow from squeeze-out is weaker due to the lack of a nuclear force which demonstrates the relative role of the momentum-dependent nuclear forces on the v_2 observable below bombarding energies of about 5 A GeV.

5. Summary

In this contribution we have explored the dependence of transverse and radial flow signals on various model inputs — that are related to the nuclear EoS — using the coupled channel RBUU model. We find that the mass distribution of the resonances included in the model plays an important role for the description of transverse flow above 1 A GeV. For the radial flow we have concentrated on the difference between the results for the flow temperature T and flow velocity β when using different EoS. However, no sizeable sensitivity to the compressibility of the EoS could be established.

On the other hand, we found that in order to reach a consistent understanding of the nucleon optical potential up to 1 GeV, the transverse mass distributions of protons at AGS energies as well as the excitation function of sideways and elliptic flow [9,43] up to 11 A GeV, the strength of the vector potential has to be reduced in the RBUU model at high relative momenta and/or densities. Otherwise, too much flow is generated in the early stages of the reaction and cannot be reduced at later phases where the Schrödinger equivalent potential is experimentally known. This constrains the parameterizations of the explicit momentum dependence of the vector and scalar mean fields U_μ and U_S at high relative momenta.

In addition, we have shown the relative role of resonance and string degrees of freedom at AGS energies. By reducing the number of degrees of freedom via high mass resonances one can build up a higher pressure and/or temperature of the ‘fireball’ which shows up in the transverse mass spectra of protons as well as in the sideways flow [27]. A possible transition from resonance to string degrees of freedom is indicated by the RBUU calculations at invariant baryon–baryon collision energies of $\sqrt{s} \approx 3.5$ GeV which corresponds to a proton laboratory energy of about 4.6 GeV. Due to Fermi motion of the nucleons in Au+Au collisions the transition from resonance to string degrees of freedom becomes smooth and starts from about 3 A GeV; at 11 A GeV practically all initial baryon–baryon collisions end up in strings, *i.e.* hadronic excitations in the continuum that decay to hadrons on a time scale of about 0.8 fm/c in their rest frame. This initial high-density *string matter* (up to $10 \rho_0$ at 11 A GeV) should not be interpreted as *hadronic matter* since it implies roughly 5 constituent quarks per fm³, which is more than the average quark density in a nucleon.

It is interesting to note that at roughly 4 A GeV in central Au+Au collisions the ratio K^+/π^+ is enhanced experimentally relative to transport calculations [44]. One might speculate that a restoration of chiral symmetry could be responsible for the softer collective response as well as enhanced strangeness fraction.

REFERENCES

- [1] K. Schertler *et al.*, *Nucl. Phys.* **A637**, 451 (1998).
- [2] C. Gale, G. Bertsch, S. Das Gupta, *Phys. Rev.* **C35**, 1666 (1987).
- [3] B. Blättel, V. Koch, A. Lang *et al.*, *Phys. Rev.* **C43**, 2728 (1991).
- [4] A. Hombach, W. Cassing *et al.*, *Eur. Phys. J.* **A5**, 157 (1999).
- [5] H. Stöcker, W. Greiner, *Phys. Rep.* **137**, 277 (1986).
- [6] H.H. Gutbrod *et al.*, *Rep. Prog. Phys.* **52**, 1267 (1989).
- [7] N. Herrmann *et al.*, *Nucl. Phys.* **A610**, 49c (1996).
- [8] W. Reisdorf, H.G. Ritter, *Ann. Rev. Nucl. Part. Sci.* **47**, 1 (1997).
- [9] P. Braun-Munzinger, J. Stachel, *Nucl. Phys.* **A638**, 3c (1998).
- [10] P. Chung *et al.*, *J. Phys. G* **25**, 255 (1999).
- [11] D. Rischke, *Nucl. Phys.* **A610**, 88c (1996).
- [12] P. Danielewicz *et al.*, *Phys. Rev. Lett.* **81**, 2438 (1998).
- [13] P.K. Sahu, A. Hombach, W. Cassing *et al.*, *Nucl. Phys.* **A640**, 493 (1998).
- [14] W. Ehehalt, W. Cassing, *Nucl. Phys.* **A602**, 449 (1996); J. Geiss, W. Cassing, C. Greiner, *Nucl. Phys.* **A644**, 107 (1998).
- [15] W. Cassing, E.L. Bratkovskaya, *Phys. Rep.* **308**, 65 (1999).

- [16] Q. Pan, P. Danielewicz, *Phys. Rev. Lett.* **70**, 2062 (1993).
- [17] T. Maruyama, W. Cassing, U. Mosel *et al.*, *Nucl. Phys.* **A573**, 653 (1994).
- [18] S.A. Bass *et al.*, *Prog. Part. Nucl. Phys.* **41**, 255 (1998); *J. Phys.* **G25**, R1 (1999).
- [19] G.Q. Li, G.E. Brown, C.H. Lee, C.M. Ko, nucl-th/9702023 (1997).
- [20] W. Cassing, V. Metag, U. Mosel, K. Niita, *Phys. Rep.* **188**, 363 (1990); W. Cassing, U. Mosel, *Prog. Part. Nucl. Phys.* **25**, 235 (1990).
- [21] S.K. Ghosh, S.C. Phatak, P.K. Sahu, *Z. Phys.* **A352**, 457 (1996).
- [22] A. Lang, B. Blättel, W. Cassing *et al.*, *Z. Phys.* **A340**, 207 (1991).
- [23] B.A. Li *et al.*, nucl-th/9904013.
- [24] S. Soff *et al.*, nucl-th/9903061.
- [25] S. Hama *et al.*, *Phys. Rev.* **C41**, 2737 (1990).
- [26] K. Weber, B. Blättel, W. Cassing *et al.*, *Nucl. Phys.* **A552**, 571 (1993).
- [27] P.K. Sahu, W. Cassing, U. Mosel, A. Ohnishi, nucl-th/9907002.
- [28] Y. Nara, N. Otuka, A. Ohnishi *et al.*, nucl-th/9904059.
- [29] Y. Nara *et al.*, *Prog. Theor. Phys. Suppl.* **129**, 33 (1997).
- [30] M. Belkacem, M. Brandstetter, S.A. Bass *et al.*, *Phys. Rev.* **C58**, 1727 (1998); L.V. Bravina *et al.*, *J. Phys.* **G25**, 351 (1999).
- [31] M. Effenberger, E.L. Bratkovskaya, U. Mosel, nucl-th/9903026.
- [32] B. Anderson, G. Gustafson, Hong Pi, *Z. Phys.* **C57**, 485 (1993).
- [33] S. Teis, W. Cassing, M. Effenberger *et al.*, *Z. Phys.* **A356**, 421 (1997).
- [34] L. Ahle *et al.*, *Phys. Rev.* **C57**, R466 (1998).
- [35] P. Crochet *et al.*, *Nucl. Phys.* **A627**, 522 (1997).
- [36] S.C. Jeong *et al.*, *Phys. Rev. Lett.* **72**, 3468 (1994).
- [37] P.J. Siemens, J.O. Rasmussen, *Phys. Rev. Lett.* **42**, 880 (1979).
- [38] M.A. Lisa *et al.*, *Phys. Rev. Lett.* **75**, 2662 (1995).
- [39] G. Poggi *et al.*, *Nucl. Phys.* **A586**, 755 (1995).
- [40] B. Hong *et al.*, *Phys. Lett.* **B407**, 115 (1997).
- [41] A. Hombach, W. Cassing, U. Mosel, *Eur. Phys. J.* **A5**, 77 (1999).
- [42] K.G.R. Doss *et al.*, *Phys. Rev. Lett.* **57**, 302 (1987).
- [43] N.N. Ajitanand *et al.*, *Nucl. Phys.* **A638**, 451c (1998).
- [44] W. Cassing, *Acta Phys. Pol.* **B29**, 3175 (1998).